DOI: 10.26599/FSHW.2026.9251127

Contents lists available at SciOpen

Food Science and Human Wellness

journal homepage: https://www.sciopen.com/journal/2097-0765

China Food Publishing Co.

Total Saponins from *Panax Japonicus* Regulate β-Oxidation in Adipocytes through the miR192-3p/GSK3β Pathway

Ning Yang [a, b, c, 1], Yuting Liu [a, d, 1], Yaqi Hu [a, b], Qianqian Yao [a, b, c], Chengfu Yuan [a, b, c*]

[a] *Hubei Key Laboratory of Tumor Microenvironment and Immunotherapy, China Three Gorges University, Yichang 443002, China*

[b] *College of Basic Medical Science, China Three Gorges University, Yichang 443002, China*

[c] *Third-grade Pharmacological Laboratory on Traditional Chinese Medicine, State Administration of Traditional Chinese Medicine, China Three Gorges University, Yichang 443002, China*

[d] *College of Medicine and Health Science, China Three Gorges University, Yichang 443002, China*

ABSTRACT: Hyperlipidemia, a major component of metabolic syndrome, poses a substantial global public health challenge. Total saponins from *Panax japonicus* C.A. Mey. (TSPJ) have been reported to improve lipid metabolism, but the underlying mechanisms are not fully understood. This study investigated whether TSPJ promote fatty acid β-oxidation in mouse and adipocyte models and explored the involvement of the microRNA-192-3p (miR-192-3p) / glycogen synthase kinase-3 beta (GSK3β) pathway. Hyperlipidemia was induced in mice using high-fat-diet (HFD), and in those mice, TSPJ reduced body weight, epididymal fat index, and serum triglyceride (TG), total cholesterol (CHO) and low-density lipoprotein cholesterol (LDL-C) levels, while increasing high-density lipoprotein cholesterol (HDL-C) and β-hydroxybutyrate (β-HB) concentrations and upregulating key β-oxidation enzymes in epididymal white adipose tissue. Cell models were created by inducing 3T3-L1 adipocytes with palmitic acid (PA), and in those cells, TSPJ decreased lipid droplet accumulation and similarly enhanced the expression of β-oxidation-related enzymes. Mechanistically, TSPJ upregulated miR-192, suppressed GSK3β expression, increased GSK3β phosphorylation at Ser9, and thereby promoted the expression of β-oxidation enzymes. Knockdown of miR-192 abrogated the effects of TSPJ on GSK3β signaling, β-oxidation, and lipid accumulation, but additional knockdown of GSK3β restored β-oxidation and attenuated lipid deposition. These findings demonstrate that TSPJ enhances mitochondrial fatty acid β-oxidation via the miR-192-3p/GSK3β pathway, supporting its potential as a therapeutic candidate for hyperlipidemia.

Keywords: total saponins from Panax japonicus; hyperlipidemia; β-oxidation; adeno-associated virus; miR-192-3p/GSK3β pathway

1. Introduction

Hyperlipidemia, characterized by elevated levels of lipids such as cholesterol and triglycerides in the blood, poses a significant global health burden[1-3]. It is a major risk factor for cardiovascular diseases (CVDs), particularly ischemic heart disease and stroke. Recent epidemiological reports highlight that CVDs remain the leading cause of death worldwide, accounting for nearly one-third of all global deaths in 2022,

[1] These authors contributed equally to this work.
***Corresponding author**
yuancf46@ctgu.edu.cn

Received 30 August 2025
Received in revised from 29 November 2025
Accepted 12 February 2026

with hyperlipidemia recognized as a primary driver of this burden[4]. Beyond its cardiovascular consequences, hyperlipidemia often coexists with obesity, diabetes, hypertension, and metabolic syndrome, thereby amplifying overall disease risk. Mechanistically, it promotes atherosclerosis through low-density lipoprotein cholesterol (LDL-C) accumulation, inflammation, and endothelial dysfunction. Its pathogenesis reflects the combined influence of genetic predisposition and lifestyle factors, and management typically combines lifestyle modification alongside pharmacological intervention tailored to disease severity and patient characteristics.

Controlling hyperlipidemia requires reestablishing systemic balance in lipid production, processing, and clearance, as the condition fundamentally arises from the dysregulation of lipid homeostasis[5, 6]. The commonly prescribed pharmacological agents for managing lipid levels involve various mechanisms of action. Statins act by inhibiting 3-hydroxy-3-methylglutaryl-coenzyme A (HMG-CoA) reductase, the primary enzyme responsible for hepatic cholesterol synthesis. This inhibition reduces intracellular cholesterol levels, which in turn stimulates the expression of LDL receptors, effectively lowering LDL-C concentrations in the bloodstream. Fibrates activate peroxisome proliferator-activated receptors (PPAR-α) to enhance the oxidation of fatty acids (FFA), thus decreasing triglyceride (TG) levels and modestly raising high-density lipoprotein cholesterol (HDL-C). Ezetimibe works by inhibiting the intestinal niemann-pick C1-like 1 (NPC1L1) transporter to reduce the absorption of dietary and biliary cholesterol. Proprotein convertase subtilisin/kexin type 9 (PCSK9) inhibitors block the PCSK9 protein, which enhances the recycling of low-density lipoprotein (LDL) receptors and significantly increases LDL clearance from the circulation. Bile acid sequestrants bind bile acids in the gut, prompting the liver to convert more cholesterol into bile acids, thus decreasing plasma cholesterol levels. Nevertheless, residual cardiovascular risk and drug intolerance in some patients underscore the need for additional lipid-modulating strategies that target complementary pathways, such as fatty acid oxidation.

Fatty acid oxidation is a key component of the lipid metabolism[7-9] and it encompasses several pathways, among which β-oxidation is the principal mechanism for energy production from straight-chain fatty acids. During β-oxidation, fatty acids are first activated in the cytoplasm by binding to coenzyme A (CoA), forming acyl-CoA in an ATP-dependent manner. The resultant acyl-CoA is then transported into the mitochondrial matrix via the carnitine shuttle system, and inside mitochondria, it undergoes a series of enzymatic reactions to yield acetyl-CoA, which enters the citric acid cycle to support cellular energy production[10-12]. Impaired β-oxidation in adipose tissue has been implicated in lipid accumulation and broader metabolic dysregulation, and enhancing β-oxidation, particularly in adipocytes, may help reduce lipid accumulation and improve metabolic profiles[13-17]. While many current treatments for hyperlipidemia focus on inhibiting lipid synthesis[18,19], greater attention to fatty acid oxidation—especially its role in cellular lipid clearance—may offer complementary benefits[20, 21].

Over the past few decades, research has unveiled the significant roles of non-coding RNAs (ncRNAs) in metabolic regulation, including microRNAs (miRNAs) and long non-coding RNAs (lncRNAs).

Researchers have found that the expression of genes related to lipid metabolism can be regulated by miR-192-3p, which in turn regulates blood lipid levels[21-23]. For both murine models and human subjects, obesity is negatively correlated with the expression level of miR-192-3p[24]. In obese patients, miR-192-3p expression is negatively correlated with serum triglyceride level and positively correlated with high-density lipoprotein (HDL)[25]. In murine models receiving a high-fat diet, the miR-192-3p expression in the adipose tissue is significantly downregulated[26].

Glycogen synthase kinase-3 beta (GSK3β) is a serine/threonine kinase[27, 28]. Recent findings highlight GSK3β as a key regulator of transcriptional control for genes involved in mitochondrial fatty acid β-oxidation pathways, as it influences cellular lipid uptake and storage dynamics through coordinated metabolic reprogramming[29-31]. In acute kidney injury models, the pharmacological inhibition of GSK3β attenuates the mitochondrial dysfunction in renal tubular epithelial cells induced by oxidative stress, specifically through the direct modulation of the mitochondrial permeability transition pore[32]. Thus, the downregulation of GSK3β leads to the restoration of lipid metabolic homeostasis[33]. Analogously, in rat ventricular cardiomyocytes, the pharmacological inhibition of GSK3β exerts a cardioprotective effect by preserving the mitochondrial membrane potential against peroxide-induced oxidative damage and restoring lipid metabolic homeostasis[34]. These findings collectively indicate that GSK3β acts as a critical regulator of β-oxidation enzyme expression and mitochondrial function, orchestrating lipid metabolism and supporting systemic lipid homeostasis.

Panax japonicus C.A. Mey. (*P. japonicus*), also referred to as “bamboo ginseng”, is a perennial herb used in traditional medicine across East Asia for its diverse pharmacological properties, including anti-inflammatory, antioxidant, and immunomodulatory effects[35]. The total saponins from *P. japonicus* (TSPJ) have been validated as a bioactive phytochemical complex that modulates dysregulated lipid metabolism and demonstrates significant therapeutic efficacy in alleviating lipid abnormalities associated with metabolic syndrome through multi-target mechanisms[36, 37]. Although TSPJ have been reported to exert lipid-lowering and metabolism-regulating effects, the molecular mechanisms underlying these actions remain partly understood. Whether TSPJ can directly enhance fatty acid β-oxidation in adipocytes has not been systematically investigated, and it is unclear whether TSPJ interact with the miR-192-3p/GSK3β axis, a pathway strongly implicated in lipid metabolic homeostasis. We previously disclosed that in mice receiving a high-fat diet, TSPJ can decrease the body weight, reduce the serum triglyceride, and improve lipolysis in the epididymal adipose tissue. In this work, we demonstrate through animal and cell models that TSPJ mitigate hyperlipidemia via the miR-192-3p/GSK3β axis.

2. Materials and methods

2.1. Extraction of TSPJ

P. japonicus was obtained from the Chunmuying Chinese Medicinal Herb Production Base in Enshi, Hubei, China and authenticated by Dr. Ding Yuan from China Three Gorges University. The identification was further verified using the World Flora Online database (https://www.worldfloraonline.org/). Voucher

specimens were preserved at the Institute of Chinese Herb Medicine, College of Medicine and Health Science, China Three Gorges University.

The rhizomes of *P. japonicus* were mechanically pulverized and extracted with 60% ethanol under reflux at a solid–liquid ratio of 1:10 (w/v; 1 kg dried powder per 10 L solvent, 3 times, 2 h each time). The combined ethanolic solution was concentrated to about 20% of the initial volume, then extracted serially with petroleum ether, ethyl acetate, and *n*-butanol. The butanolic extract was loaded on a macroporous resin column (D101, Tianjin Pesticide Factory, Tianjin, China), which was washed with water until the eluent became colorless. The column was then flushed with 60% ethanol, and the eluate was concentrated under reduced pressure and freeze-dried to give a light-yellow powder as TSPJ[38]. According to high performance liquid chromatography (HPLC, Thermo Fisher Scientific, Shanghai, China), the saponin content of TSPJ was 83.48%. The main components of TSPJ were further characterized by following the previously reported method[39]. Briefly, a gradient elution was performed using acetonitrile (mobile phase A) and 0.1% phosphoric acid in water (mobile phase B). The proportion of A was programmed as follows: 5–19% for 0–15 min, 19–23% for 15–25 min, 23–32% for 25–40 min, 32–70% for 40–60 min, followed by an isocratic hold at 70% A for an additional 20 min. The injection volume was 10 μL, the flow rate was set to 1.0 mL/min, the column was maintained at 30 °C, and detection was carried out at 205 nm. Peak identities were assigned by comparison with an authentic mixed reference standard containing multiple saponins (National Institutes for Food and Drug Control, China). Based on retention time matching, the major peaks in the TSPJ chromatogram were assigned to Chikusetsu saponin V (CS-V), Chikusetsu saponin IV (CS-IV), Chikusetsu saponin IVa (CS-IVa), 20(*S*)-ginsenoside Rh1 (Rh1), ginsenoside Rg1 (Rg1), 20(*S*)-ginsenoside Rg2 (Rg2), and ginsenoside Rf (Rf). The same batch of TSPJ characterized in the previous study was used in the present experiment[39].

2.2. Animal experiments

Male specific pathogen-free (SPF) C57BL/6J mice (5 weeks old, 18–20 g) were sourced from the Laboratory Animal Center at China Three Gorges University (license: SCXK [Hubei] 2022-0061; Hubei, China). The mice were raised in a standard environment, i.e., 22 ± 2 °C, 60% ± 5% humidity, 12 h/12 h diurnal cycle, and had unrestricted access to food and water. After acclimation for one week, they were randomly allocated into eight groups, each containing 8 mice (Table 1).

Table 1. Experimental groups of mouse models.

Number	Name	Diet	TSPJ‡ (mg/(kg·d))	miR-192 knockdown
N1	ND*	ND	0	N/A**
N2	HFD†	HFD	0	
N3	TSPJ-L	HFD	25	
N4	TSPJ-H	HFD	50	
N5	AAV-NC inh.§,‖,¶	HFD	0	No
N6	AAV-NC inh.-TSPJ	HFD	50	No
N7	AAV-miR192 inh.	HFD	0	Yes
N8	AAV-miR192 inh.-TSPJ	HFD	50	Yes

* ND: normal diet, † HFD: high-fat diet, ‡ TSPJ: total saponins from *panax japonicus*, § AAV: adeno-associated virus, ‖ NC: negative control, ¶ inh.: inhibitor, ** N/A: not applicable.

The mice in Group N1 received a normal diet, and all other mice received an high-fat-diet (HFD) (Table S1). The mice in Groups N3 and Group N4 received TSPJ by gavage (25 and 50 mg/kg·d, respectively), while those in Groups N1 and N2 received the equivalent volume of 0.5% w/v carboxymethyl cellulose sodium (CMC-Na; Aladdin, Shanghai, China). The mice in Groups N5–N8 were raised initially with a normal diet and switched to HFD from week 7. Starting from week 8, the mice in Groups N6 and N8 were given 50 mg/kg·d of TSPJ by gavage, while those in Groups N5 and N7 were given the same volume of 0.5% w/v CMC-Na. On week 21, according to the assignment described in Table 1, the mice were injected with an adeno-associated virus (AAV; Genepharma Co., Ltd., Shanghai, China; 1×10^{12} VG/mL) carrying either an empty vector (AAV-NC inh.) or a miR-192 inhibitor (AAV-miR192 inh.) directly into the epididymal adipose tissue.

On week 24, the mice were sacrificed in accordance with institutional and national guidelines. They were first anesthetized with an intraperitoneal injection of 20% urethane and 10 mg/kg xylazine and then euthanized by an overdose of the same anesthetic. Blood samples and adipose tissues were collected immediately and stored at −80 °C before use.

The quality of the animals used in this study was verified by the Center for Disease Control and Prevention of Hubei Province. All experimental procedures in this study involving animals were conducted in strict compliance with the Guidelines for the Care and Use of Laboratory Animals outlined by the National Institutes of Health. This study was approved by the Animal Protection and Utilization Management Committee of China Three Gorges University (approval No. 2019080D-1).

2.3. Cell experiments

Mouse 3T3-L1 preadipocytes, obtained from the Cell Resource Center at the Shanghai Institutes for Biological Sciences, Chinese Academy of Sciences, were cultured in Dulbecco's Modified Eagle Medium (DMEM) with 10% fetal bovine serum (FBS). They were seeded into culture dishes at about 45% cell density and induced to differentiate in a complete culture medium supplemented with 10 μg/mL insulin (Kerui Biotechnology, Wuhan, China), 0.5 μM 3-isobutyl-1-methylxanthine (MeilunBio, Dalan, China), 10 μM indoleacetic acid (Kerui Biotechnology, Wuhan, China), 1 μM dexamethasone (Kerui Biotechnology, Wuhan, China), and 1 μM rosiglitazone (Kerui Biotechnology, Wuhan, China). The mature adipocytes were collected and allocated into the eight experimental groups specified in Table 2.

Table 2. Experimental groups of cell models.

Number	Name	Palmitic acid	TSPJ‡ (μg/mL)	miR-192 knockdown	GSK3β knockdown
C1	NC*	No	0	N/A**	
C2	PA†	Yes	0		
C3	PA-TSPJ-L	Yes	25		
C4	PA-TSPJ-H	Yes	50		
C5	NC inh. + siNC§,‖	Yes	50	No	No
C6	NC inh. + siGSK3β¶	Yes	50	No	Yes
C7	miR192 inh. + siNC	Yes	50	Yes	No
C8	miR192 inh. + siGSK3β	Yes	50	Yes	Yes

* NC: negative control, † PA: palmitic acid, ‡ TSPJ: total saponins from *panax japonicus*, § inh.: inhibitor, ‖ siNC: small interfering negative control RNA, ¶ siGSK3β: small interfering RNA targeting GSK3β, ** N/A: not applicable.

For Groups C1–C4, the cells were first cultured in a cell incubator under 5% CO_2 at 37 °C for 24 h in (1) complete medium, (2) complete medium containing 500 μmol/L palmitic acid (PA, Sigma-Aldrich, St. Louis, USA), and (3) complete medium containing 25 μg/mL TSPJ, (4) complete medium containing 50 μg/mL TSPJ. Afterwards, for all groups, the medium was replaced with the complete medium containing 500 μmol/L PA, and the cells were cultured for another 24 h.

For Groups C5–C8, the cells were first cultured in the complete medium with 500 μmol/L PA for 48 h. The collected cells were re-seeded in six-well plates until the confluence reached 70%–80% and used for subsequent experiments. To carry out siRNA transfection, siRNA (100 pmol; Beyotime, Shanghai, China) and Lipo8000 (4 μL; Beyotime, Shanghai, China) were each diluted in serum- and antibiotics-free DMEM (125 μL). The two solutions were incubated at room temperature for 10 min before they were mixed, and the mixture was maintained at room temperature for another 20 min. The cells awaiting transfection were refreshed in serum- and antibiotics-free DMEM before the addition of the transfection mixture, and after incubation at room temperature for 6 h, the medium was replaced with a complete medium containing 50 μg/mL TSPJ. The cells were then cultured further for 48 h.

2.4. H&E staining

The adipose tissue was fixed in 4% paraformaldehyde and embedded in paraffin wax before being sectioned into 4 μm slices using a microtome. The paraffin was removed with xylene, and the sections were rehydrated using a descending ethanol gradient. Subsequently, the slices were stained with hematoxylin and eosin (H&E; Sigma-Aldrich, St. Louis, USA), dehydrated using an ascending ethanol gradient, and sealed with a mounting medium. Finally, the stained sections were observed and photographed using an optical microscope to determine the pathological changes of the adipose tissue.

2.5. Immunohistochemistry

Thin slices of the adipose tissue were prepared as described in Section 2.4. The rehydrated tissue slices were heated in citrate buffer (pH = 6.0) at 95–100 °C for 10–20 min for antigen repair and then treated with 3% H_2O_2 in phosphate-buffered saline (PBS) for 10–15 min to block endogenous peroxidase activity. The tissue sections were then incubated with the primary antibody at 4 °C overnight, washed with PBS three times, incubated with the secondary antibody at room temperature for 1 h, rinsed with PBS three times, and stained with diaminobenzidine (DAB; Kerui Biotechnology, Wuhan, China). The cell nuclei were counterstained with hematoxylin (Kerui Biotechnology, Wuhan, China) to enhance contrast. Finally, the stained sections were sealed with a neutral resin, examined under an optical microscope, and photographed.

2.6. Oil red O staining

The 3T3-L1 preadipocytes were washed with PBS and fixed with 4% paraformaldehyde at room temperature for 30 min. After fixation, the cells were thoroughly washed with PBS, stained with oil red O (Kerui Biotechnology, Wuhan, China) at room temperature for 20 min, and washed thoroughly with PBS again to remove the excess dye. Lipid droplets were then observed and photographed under a light

microscope. Subsequently, the oil red O stain was eluted with isopropyl alcohol, and the absorbance of the extracted dye was measured at 510 nm using a microplate reader.

2.7. BODIPY staining

The cells were fixed with 4% paraformaldehyde at room temperature in the dark for 30 min, washed thoroughly with PBS, stained with BODIPY (Invitrogen, CA, USA) at room temperature for 30 min, rinsed with PBS, then stained with 4′,6-diamidino-2-phenylindole (DAPI; Servicebio, Wuhan, China) for 5 min. The lipid droplets were observed and photographed under a fluorescence microscope.

2.8. Western blot

Proteins were extracted by homogenizing tissue samples or lysing cell samples in RIPA buffer (Applygen Technologies, Beijing, China). The lysates were then centrifuged at 12000*g* and 4 °C for 20 min, and the supernatant containing the protein extract was carefully collected. The protein concentration was determined using the BCA assay (Applygen Technologies, Beijing, China). The protein extract was boiled in RIPA buffer for 10 min to denature the protein, and an equal amount of protein was separated by sodium dodecyl sulfate polyacrylamide gel electrophoresis (SDS-PAGE) and transferred to polyvinylidene fluoride (PVDF) membranes (Kerui Biotechnology, Wuhan, China). The PVDF membranes loaded with the proteins were blocked with 5% skimmed powder milk, shaken at 30 rpm at room temperature for 1 h, and incubated at 4 °C overnight with the following primary antibodies: CPT1a (1:2000, ABclonal, Wuhan, China), ECH (1:2000, ABclonal, Wuhan, China), Anti-GSK3β (1:1000, Wanleibio, Shenyang, China), Anti-p-GSK3β^{Ser9} (1:2000, Wanleibio, Shenyang, China), β-actin (1:100000, ABclonal, Wuhan, China). Afterwards, the membranes were rinsed with Tris-buffered saline containing Tween 20 (TBST) three times and incubated with the appropriate secondary antibody at room temperature for 2 h. The protein bands were visualized using an electrochemiluminescence imaging system (Bio-rad, Hercules, CA, USA) and quantitatively analyzed using ImageJ. The internal reference was β-actin.

2.9. Real-time PCR

Total RNA was extracted using TRIzol (Invitrogen, Waltham, MA, USA) and reverse-transcribed into cDNA using a reverse transcription kit (Vazyme, Nanjing, China). The PCR amplification was carried out on a qPCR system (Applied Biosystems, Waltham, MA, USA) using SYBR® Premix Ex Taq (2x) (Vazyme, Nanjing, China) and appropriate primers (Table S2). The following protocol was applied: Pre-denaturation at 95 °C for 10 min, annealing at 60 °C, then 40 cycles of amplification (5 s at 95 °C and 30 s at 60 °C). The relative expression level of the target gene was determined using the $2^{-\Delta\Delta Ct}$ method, and *β-actin* was the internal control.

2.10. Statistical analysis

All statistical analyses were performed using SPSS 21.0. Data are presented as the mean ± standard error of the mean (SEM) and visualized using GraphPad Prism 10.0. For comparisons among multiple groups, one-way ANOVA followed by Tukey's post hoc test was used when the data were normally

distributed and the variance was homogeneous. If normality or variance homogeneity was not met, the Kruskal–Wallis test and the Dunn's multiple comparisons test were applied. Differences were considered statistically significant when $P < 0.05$.

3. Results

3.1. TSPJ enhanced β-oxidation in the adipocytes of HFD-induced mice

To investigate the effects of TSPJ on β-oxidation, C57BL/6J mice were induced with HFD to establish an obesity model for the study. After 6 weeks of feeding, compared to the mice receiving a normal diet, the mice receiving HFD had significantly elevated body weight (Fig. 1A). At the end of the experiment (i.e., 16 weeks of feeding in total), the HFD-induced mice had significantly lower body weight and the epididymal fat index if they received TSPJ compared to those that did not (Fig. 1A). According to H&E staining, the epididymal white adipose tissue (eWAT) of the HFD-induced mice had a significantly larger adipocyte area, lower cell density per unit area, and disorganized cellular arrangement (Fig. 1B), but these anomalies were attenuated by TSPJ (Fig. 1B). The TSPJ treatment also significantly decreased the serum levels of TG, CHO, and LDL-C, and increased the serum level of HDL-C (Fig. 1C). In addition, TSPJ reduced the serum level of free FFA and increased that of β-HB, which is a key β-oxidation metabolite (Fig. 1D). When the mice received TSPJ, the mRNA expressions of key β-oxidation enzyme-related genes in the epididymal adipose tissue increased, including carnitine palmitoyltransferase 1A (CPT1a), carnitine-acylcarnitine translocase (CACT), acyl-CoA dehydrogenase medium chain (ACADM), and enoyl-CoA hydratase (ECH) (Fig. 1E), and the protein expression of ECH and CPT1α also increased (Fig. 1F). That is, TSPJ strengthened β-oxidation in the adipocytes of HFD-induced mice and ameliorated hyperlipidemia.

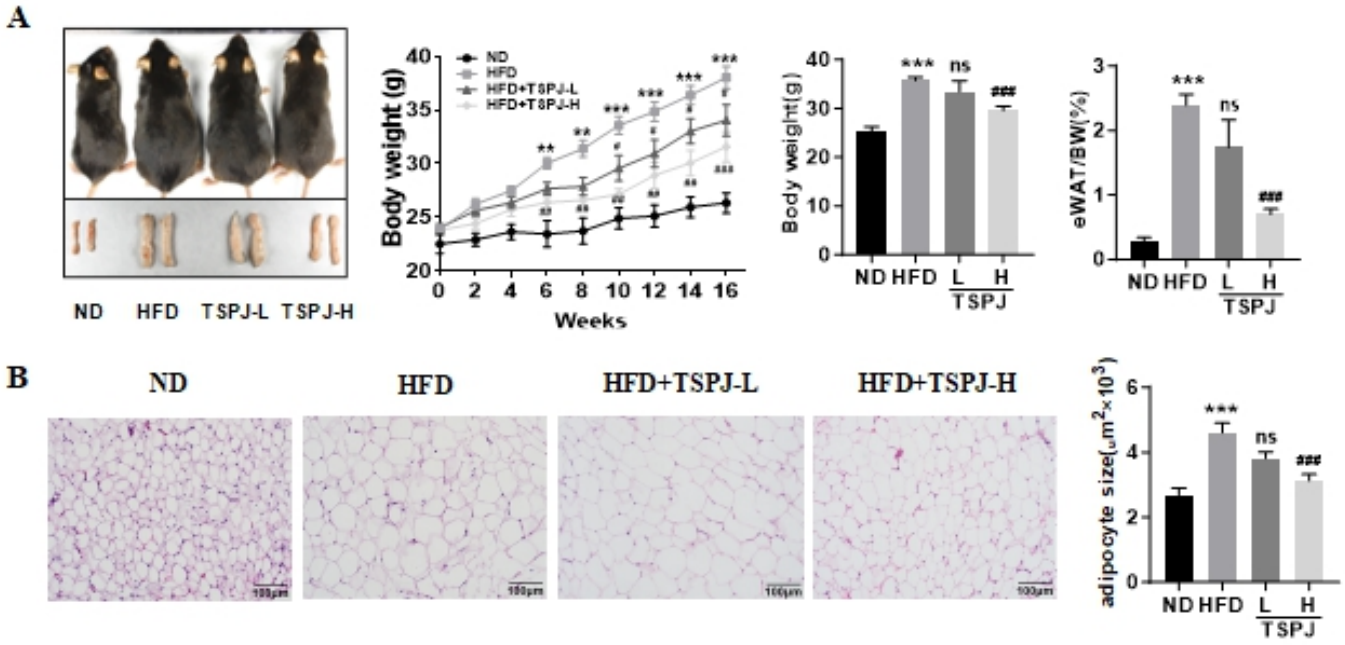

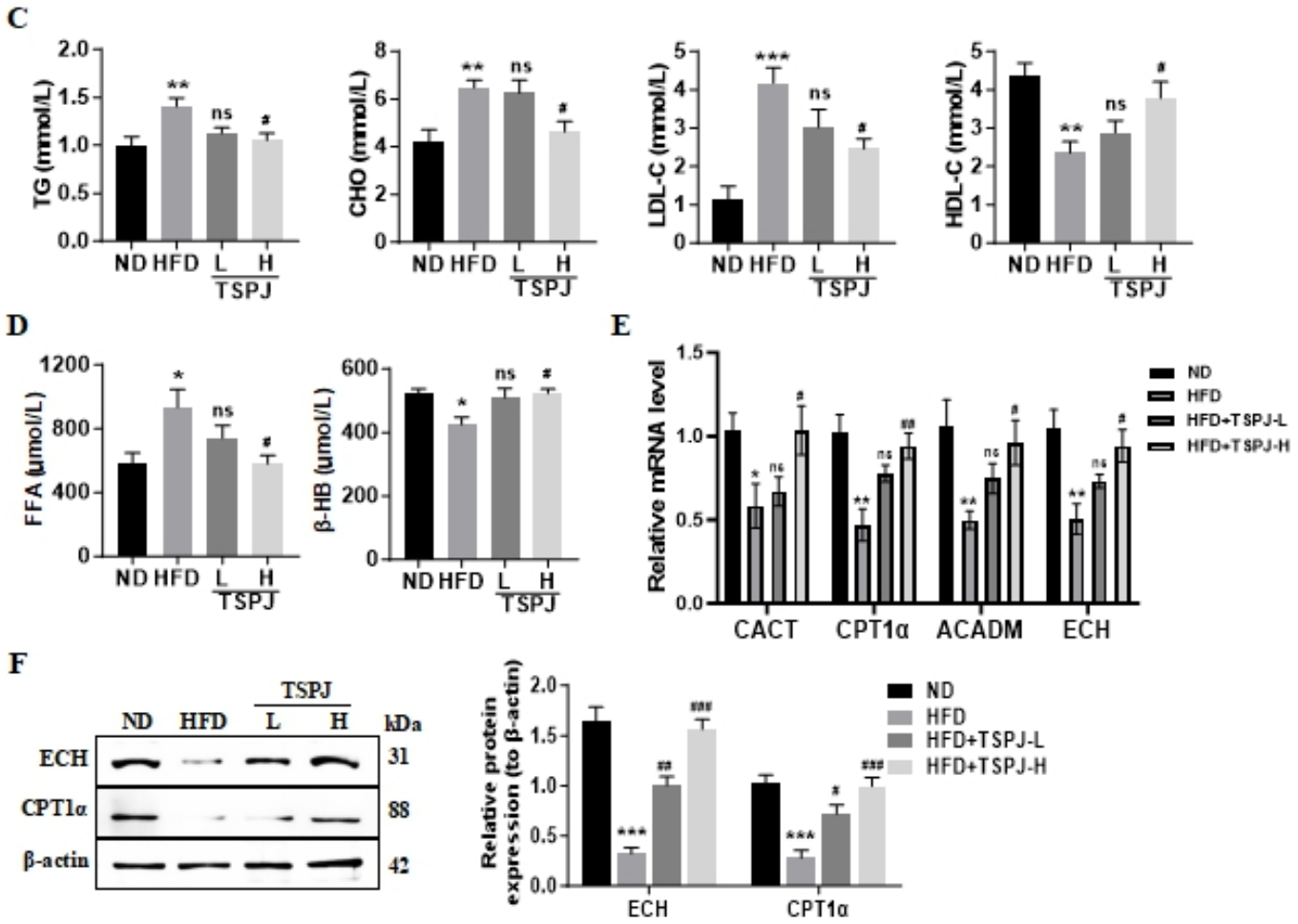

Fig. 1. Effects of TSPJ on the β-oxidation in adipocytes and the lipid profiles of HFD-induced mice. (A) Changes in body weight and epididymal fat. (B) H&E staining of epididymal fat. (C) The serum levels of TG, CHO, LDL-C, and HDL-C. (D) The serum levels of FFA and β-HB. (E) The mRNA expressions of CACT, CPT1α, ACADM, and ECH in epididymal fat. (F) The protein levels of CPT1α and ECH in epididymal fat. Data are expressed as mean ± SEM (n = 8). ** $P < 0.01$, *** $P < 0.001$, compared with the ND group; $^{\#\#}$ $P < 0.01$, $^{\#\#\#}$ $P < 0.001$, compared with the HFD group; ns, not significant.

3.2. TSPJ enhanced β-oxidation in PA-induced 3T3-L1 adipocytes

A hypertrophic cell model was established by treating mature 3T3-L1 adipocytes with PA. In the adipocytes, the lipid droplets became larger and aggregated due to PA stimulation, but with the TSPJ treatment, the accumulation of lipid droplets was reduced (Fig. 2A). The BODIPY staining also revealed that TSPJ reduced the accumulation of lipid droplets in the adipocytes (Fig. 2B). The mRNA expression levels of the genes of key β-oxidation enzymes (CACT, CPT1α, ACADM, and ECH) were decreased in PA-induced adipocytes (Fig. 2C), but the TSPJ treatment increased these mRNA expressions and elevated the protein levels of CPT1α and ECH (Fig. 2D). Therefore, in the adipocytes stimulated by PA, TSPJ reduced lipid accumulation and enhanced β-oxidation.

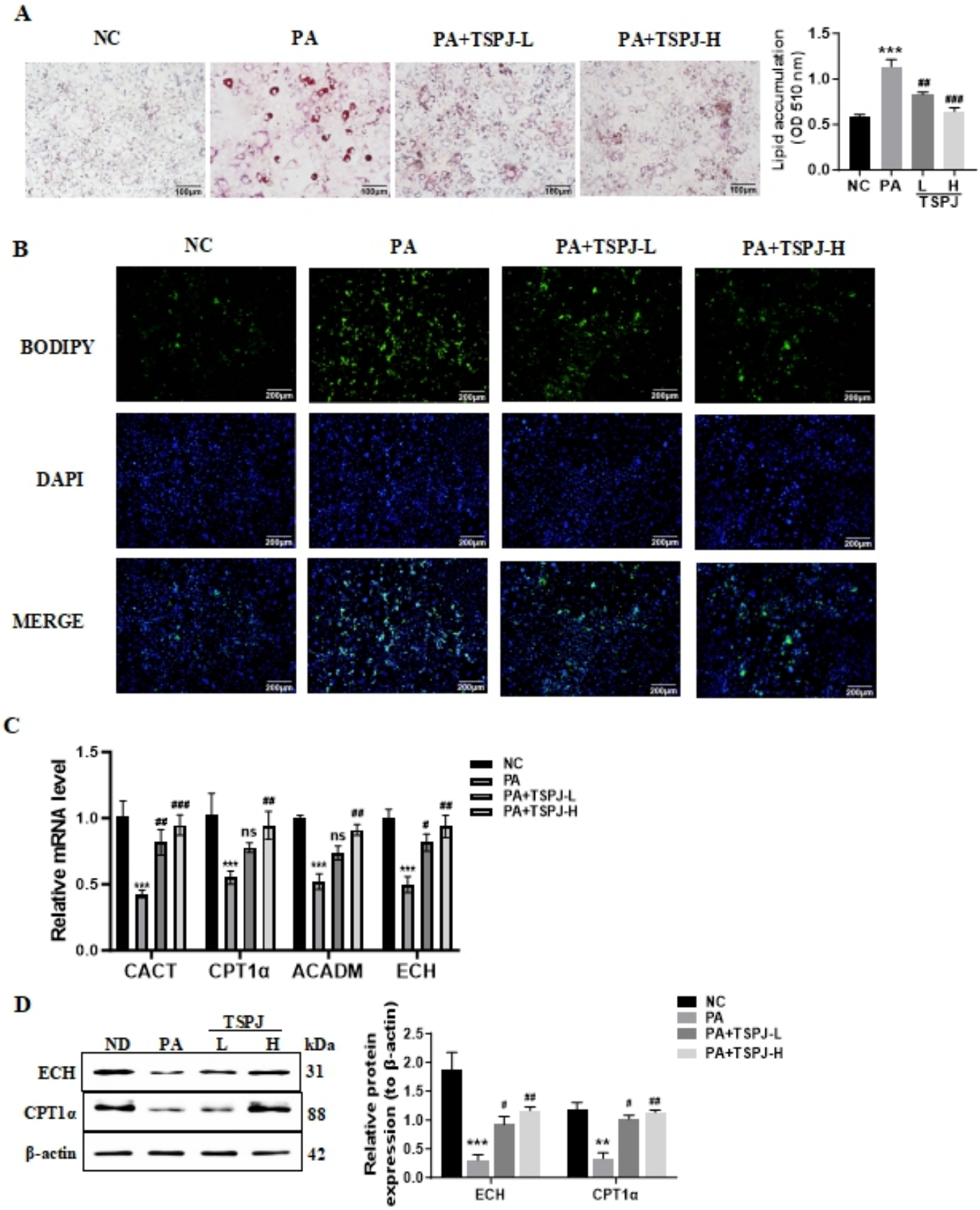

Fig. 2. Effects of TSPJ on lipid accumulation and β-oxidation in PA-induced adipocytes. (A) Oil red O staining images and corresponding OD measurements. (B) BODIPY (green) and DAPI (blue) staining images. (C) The mRNA expressions of CACT, CPT1α, ACADM, and ECH. (D) The protein levels of CPT1α and ECH. Data are expressed as mean ± SEM (n = 3). ** $P < 0.01$, *** $P < 0.001$, compared with the NC group; $^{\#\#}$ $P < 0.01$, $^{\#\#\#}$ $P < 0.001$, compared with the PA treatment group; ns, not significant.

3.3. TSPJ improved β-oxidation in HFD-induced mice by promoting miR-192 expression

It has been reported that miR-192 regulates lipid homeostasis by attenuating blood lipid accumulation and facilitating fatty acid oxidation. In the eWAT of the mouse models, the mRNA levels of miR-192 were reduced significantly by HFD and increased by TSPJ (Fig. 3A). Mouse models with miR-192 knockdown were created using the adeno-associated virus serotype GP-1 (AAV-GP-1) vector (Fig. 3B) according to the assignments outlines in Section 2.2 (Fig. 3C). According to the in vivo imaging performed three weeks post-injection, the AAV transduction was predominantly localized in the eWAT (Fig. 3D). The expression of miR-192 in the eWAT was significantly lower if the virus carried the miR-192 inhibitor instead of the negative control (Fig. 3E). The results validated the successful generation of the mouse models with miR-192 knockdown.

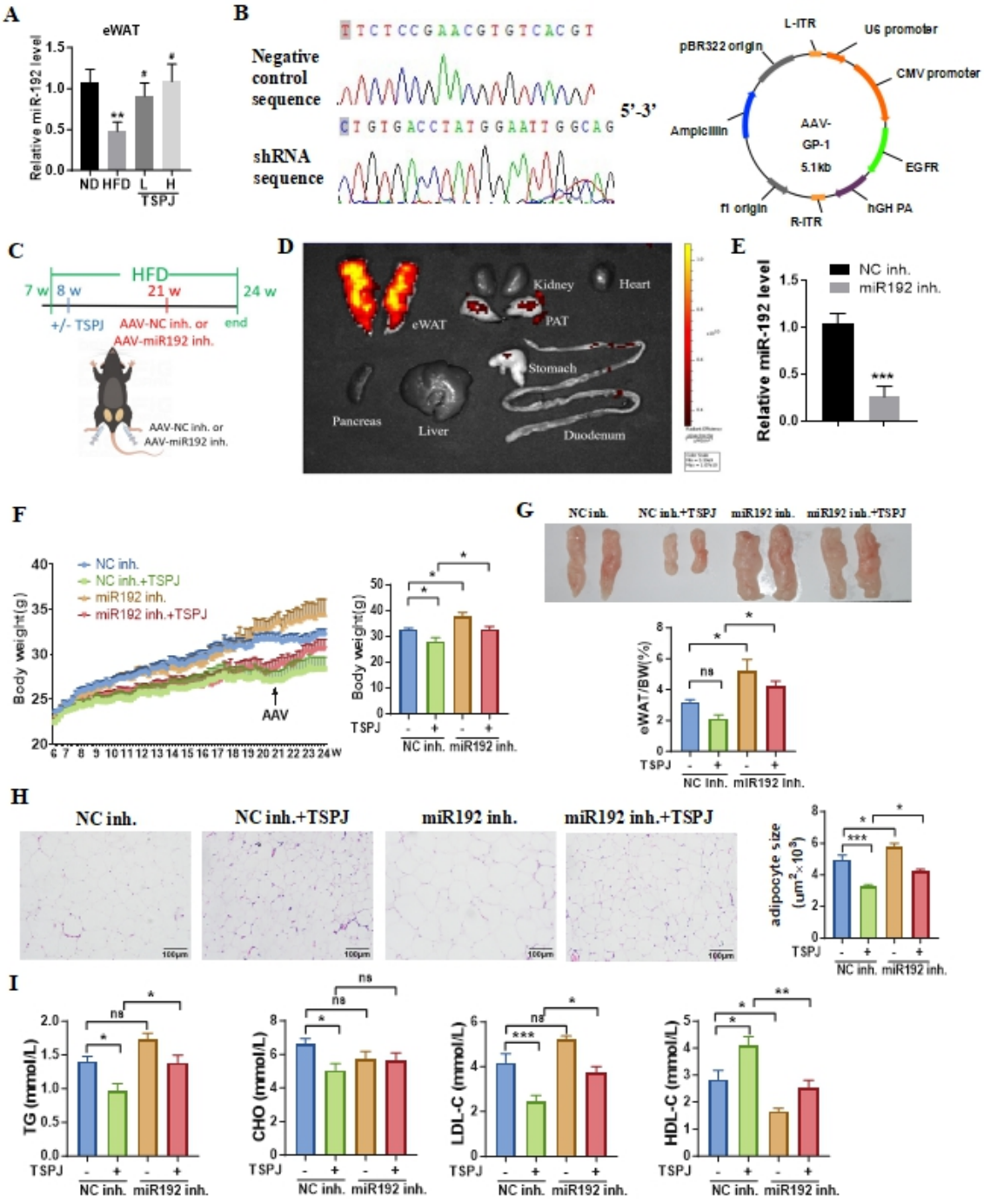

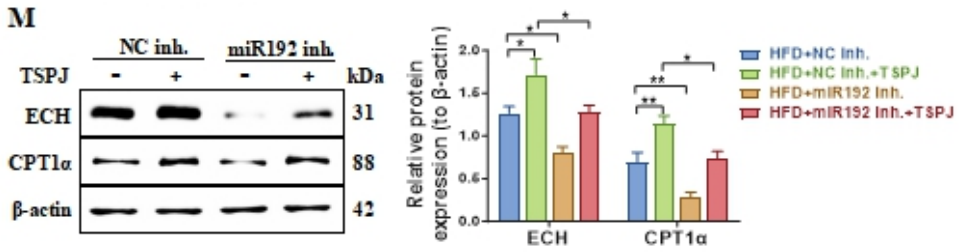

Fig. 3. Effects of TSPJ on β-oxidation in HFD-induced mice with miR-192 knockdown. (A) mRNA expression of miR-192 in eWAT. (B) Sequences of the miR-192 inhibitor and the negative control, and the construction of the plasmids. (C) Experimental setup of mouse models. (D) Efficiency of AAV transduction across organs. (E) The effects of TSPJ on the body weight of mice with miR-192 knockdown. (F) Images of the eWAT and ratio of eWAT weight to body weight. (G) H&E staining of epididymal fat. (H) TG, CHO, LDL-C, and HDL-C. (I) FFA. (J) β-HB. (K) The mRNA expressions of CACT, CPT1α, ACADM, and ECH in epididymal fat. (L) Protein levels of CPT1α and ECH in epididymal fat. Data are expressed as mean ± SEM (n = 8). * $P < 0.05$, ** $P < 0.01$, *** $P < 0.001$; ns, not significant.

Compared to the mice that received an injection of the NC inhibitor and did not consume TSPJ (Group N5), those that also got an injection of the NC inhibitor but took TSPJ (Group N6) had a lower body weight, whereas those that got an injection of the miR-192 inhibitor but did not take TSPJ (Group N7) had a higher body weight. Compared to Group N6, the mice that both got an injection of the miR-192 inhibitor and took TSPJ (Group N8) had a higher body weight (Fig. 3F). The same pattern applied to the epididymal fat index (Fig. 3G). According to H&E staining (Fig. 3H), the mice in Group N7 had swollen and deformed adipocytes compared to Group N5, and those in Group N8 (miR-192 inh. + TSPJ) had larger adipocytes than the mice in Group N6 (NC inh. + TSPJ). According to the serum analysis (Fig. 3I), compared to the mice in Group N5, those in Group N6 had lower TG, TC, and LDL-C levels along with increased levels of HDL-C. In contrast, Group N7 had an appreciable rise in TG and LDL-C and a reduction in HDL-C than Group N5. Compared to Group N6, Group N8 had higher TG and LDL-C and lower HDL-C levels. The data indicated that TSPJ ameliorated hyperlipidemia in HFD mice in a miR-192-dependent manner.

Fig. 3J,K shows that relative to Group N5, Group N6 had lower FFA and higher β-HB levels in serum, whereas Group N7 had elevated FFA and reduced β-HB. Compared to Group N6, Group N8 had higher FFA and lower β-HB. Fig. 3L shows that the mRNA expressions of the genes of key β-oxidation enzymes (CACT, CPT1α, ACADM, and ECH) were upregulated if the mice received TSPJ (Group N6 vs Group N5), while miR-192 knockdown reversed the effect of TSPJ (Group N6 vs Group N8). The protein levels of CPT1α and ECH exhibited the same pattern (Fig. 3M). It could be inferred that TSPJ promoted β-oxidation in the epididymal fat of HFD mice by upregulating miR-192 expression.

3.4. TSPJ improved β-oxidation in 3T3-L1 cells by increasing miR-192 expression

Fig. 4A verifies the successful creation of the in vitro model with miR-192 knockdown, as transfecting the 3T3-L1 cells with the miR-192 inhibitor reduced miR-192 expression significantly. Fig. 4B shows that the miR-192 expression was further decreased by PA induction but recovered partly by the TSPJ treatment. According to H&E staining (Fig. 4C), with the TSPJ treatment, the count and size of lipid droplets in the 3T3-L1 cells decreased significantly, and the OD values dropped. In contrast, the miR-192 knockdown resulted in enlarged and aggregated lipid droplets and caused a significant increase in the OD values. The

BODIPY staining (Fig. 4D) revealed that TSPJ led to a significant decrease in the count of lipid droplets but miR-192 knockdown markedly increased the number of lipid droplets. Fig. 4E shows that the mRNA expressions of the genes of key β-oxidation enzymes (CACT, CPT1α, ACADM, and ECH) were significantly increased after TSPJ treatment but decreased upon miR-192 knockdown, and the same trend was observed for the protein levels of CPT1α and ECH (Fig. 4F). Thus, TSPJ enhanced β-oxidation in PA-induced adipocytes by upregulating miR-192.

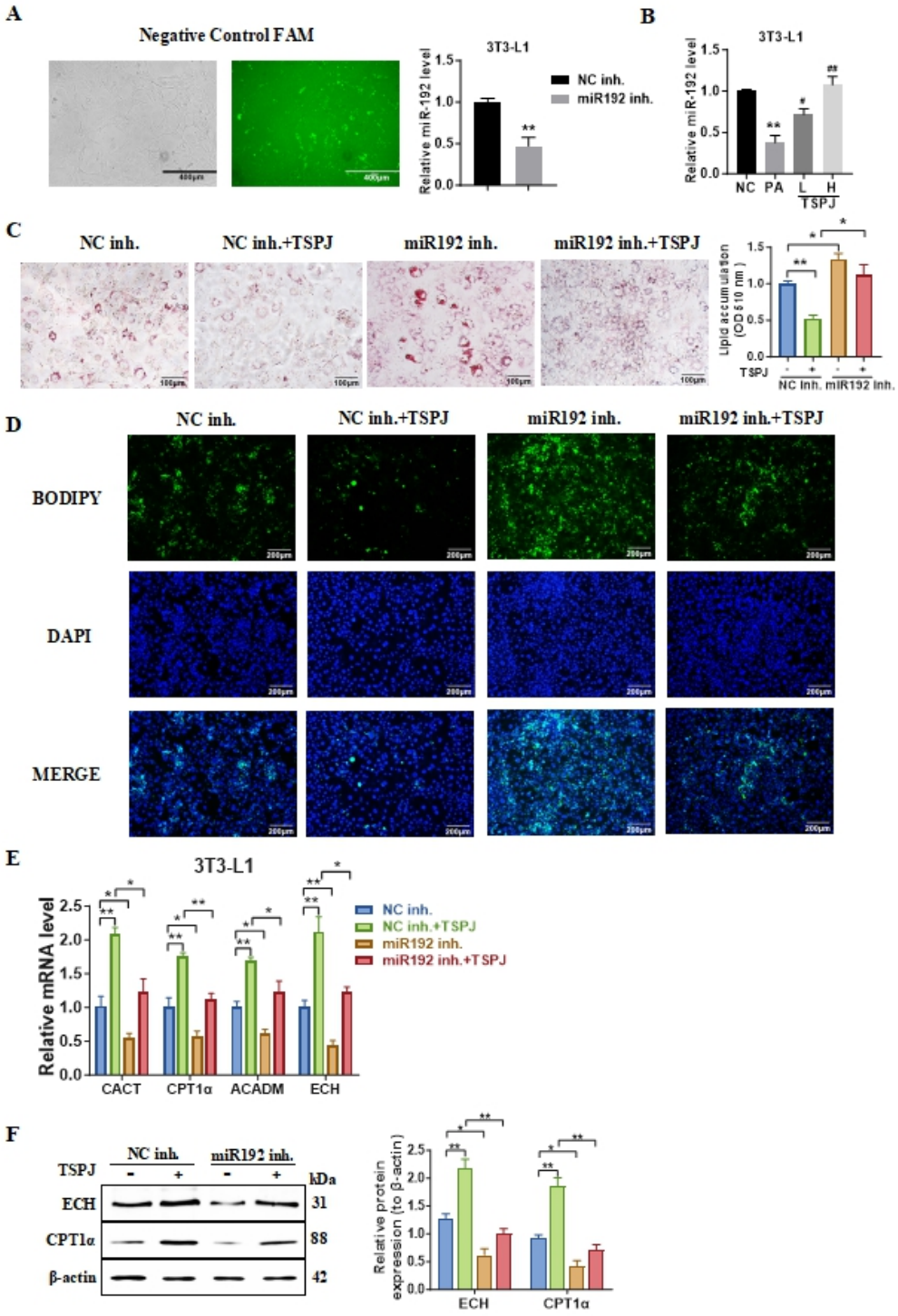

Fig. 4. Effects of TSPJ on β-oxidation in PA-induced 3T3-L1 cells with miR-192 knockdown. (A) Efficacy of the miR-192 inhibitor. (B) The expression of miR-192 in 3T3-L1 cells receiving different treatments. (C) Oil red O staining images and OD values. (D) BODIIPY staining. (E) The mRNA expressions of CACT, CPT1α, ACADM, and ECH. (F) The protein levels of CPT1α and ECH. Data are expressed as mean ± SEM (n = 8). * $P < 0.05$, ** $P < 0.01$, *** $P < 0.001$; ns, not significant.

3.5. TSPJ regulated GSK3β expression and phosphorylation via miR-192 in HFD mice

Fig. 5A shows that, based on the bioinformatic predictions from miRWalk, miRDB, and TargetScan, there are 221 candidate genes regulated by miR-192. The effect of TSPJ on their mRNA expression in eWAT was then examined. The mRNA expression of GSK3β was upregulated by HFD significantly (Fig. 5B) and inversely correlated with miR-192 (Fig. 5C). Fig. 5D shows that the HFD increased the protein levels of GSK3β and decreased those of p-GSK3β^{Ser9}, whereas TSPJ had the opposite impact. The immunohistochemical staining results further verified that TSPJ suppressed GSK3β expression and enhanced its phosphorylation in the eWAT (Fig. 5E).

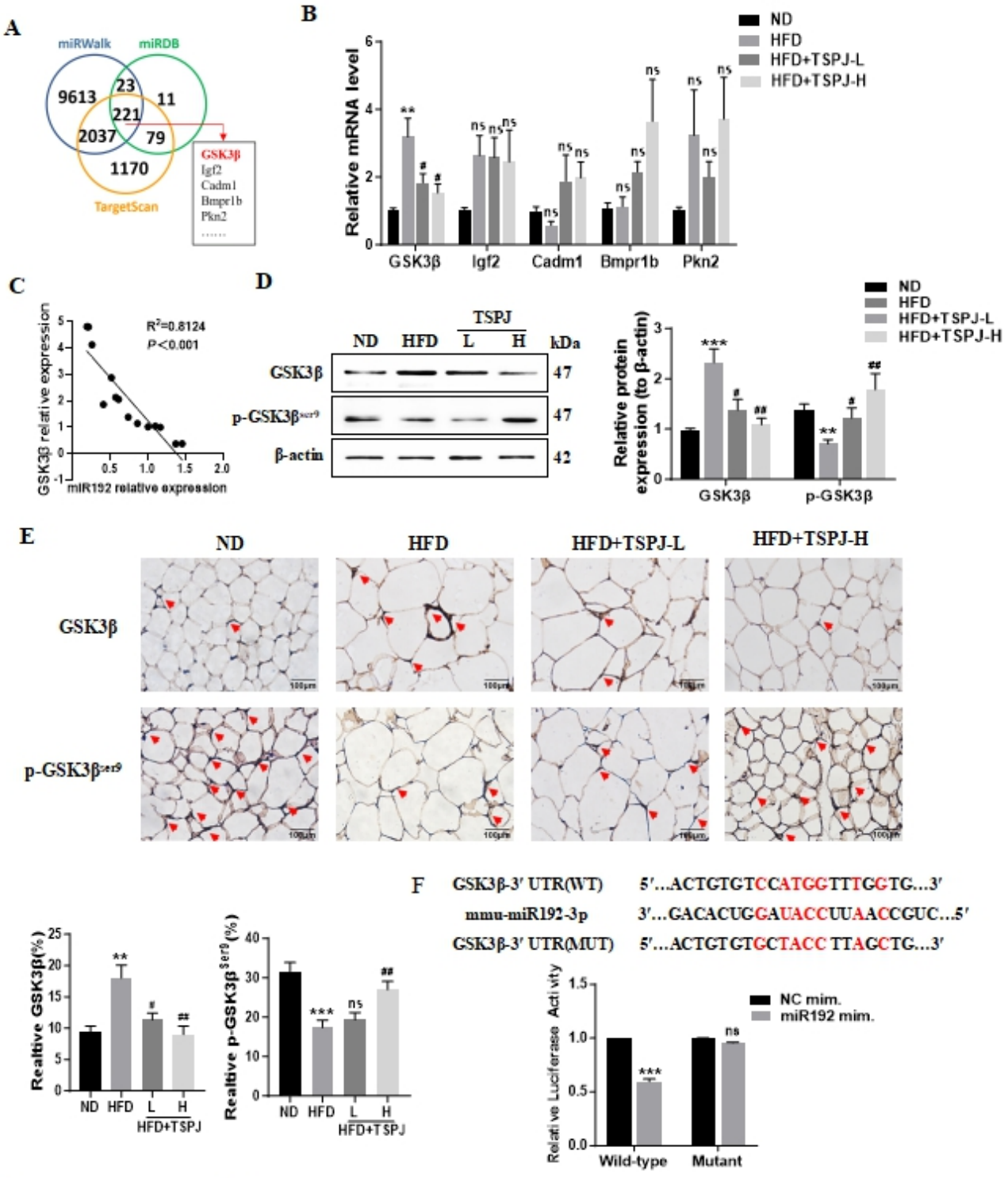

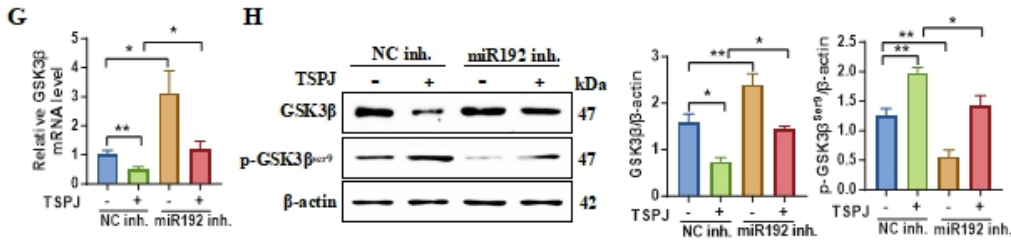

Fig. 5. TSPJ regulate the expression and phosphorylation of GSK3β in HFD-induced mice via miR-192. (A) Prediction of the target gene of miR-192. (B) The expressions of the possible downstream genes of miR-192 in eWAT. (C) Correlation between miR-192 and the mRNA expression of GSK3β. (D) Western blot and (E) IHC assays of the expression of GSK3β and p-GSK3β^{Ser9}. (F) Binding sites between miR-192 and GSK3β, and construction of the mutant sequence. (G) mRNA expression of GSK3β. (H) Western blot detections of GSK3β and p-GSK3β^{Ser9}. Data are expressed as mean ± SEM (n = 8). * $P < 0.05$, ** $P < 0.01$, *** $P < 0.001$; ns, not significant.

To determine if miR-192 directly targeted GSK3β, we identified complementary base sequences between miR-192 and GSK3β (Fig. 5F). The wild-type (WT) and mutant (MUT) plasmids of GSK3β-3'UTR were constructed accordingly and transfected into 3T3-L1 cells. The miR-192 mimic significantly decreased the luciferase activity in the WT group but had no effect on the MUT group (Fig. 5F). Therefore, miR-192 must have negatively regulated GSK3β. Fig. 5G shows that, among the mice in Group N5–N8, the TSPJ treatment reduced the mRNA expression of GSK3β (Group N6 vs Group N5), but the reduction was reversed if the mice also received an injection of the miR-192 inhibitor (Group N8 vs Group N6). Fig. 5H shows that TSPJ decreased the protein levels of GSK3β and increased the protein levels of p-GSK3β^{Ser9}, whereas miR-192 knockdown had the opposite effect on the mice receiving TSPJ. It could be inferred that TSPJ upregulated the miR-192 expression in HFD mice to inhibit the expression of GSK3β and enhance the phosphorylation of GSK3β.

3.6. TSPJ promoted β-oxidation by up-regulating miR-192 and inhibiting GSK3β expression

Fig. 6A shows that in the cell models, PA increased the mRNA expression of GSK3β, whereas TSPJ reverted the effects of PA. The PA induction significantly increased the protein levels of GSK3β and decreased the protein levels of p-GSK3β^{Ser9}, but these changes were moderated by TSPJ (Fig. 6B). The mRNA expression of GSK3β was decreased by TSPJ and increased by miR-192 knockdown (Fig. 6C). Fig. 6D shows that TSPJ decreased the protein levels of GSK3β and increased its phosphorylation, whereas miR-192 knockdown had the opposite influence. Hence, in adipocytes, TSPJ suppressed GSK3β expression and enhanced its phosphorylation by upregulating miR-192.

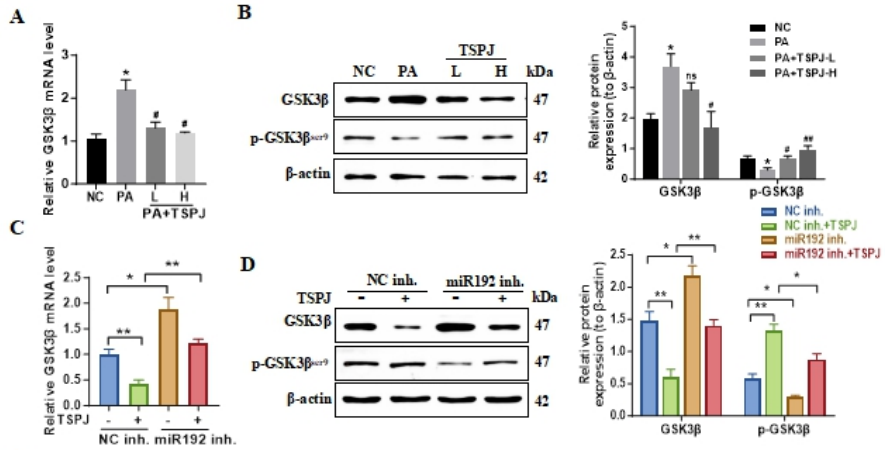

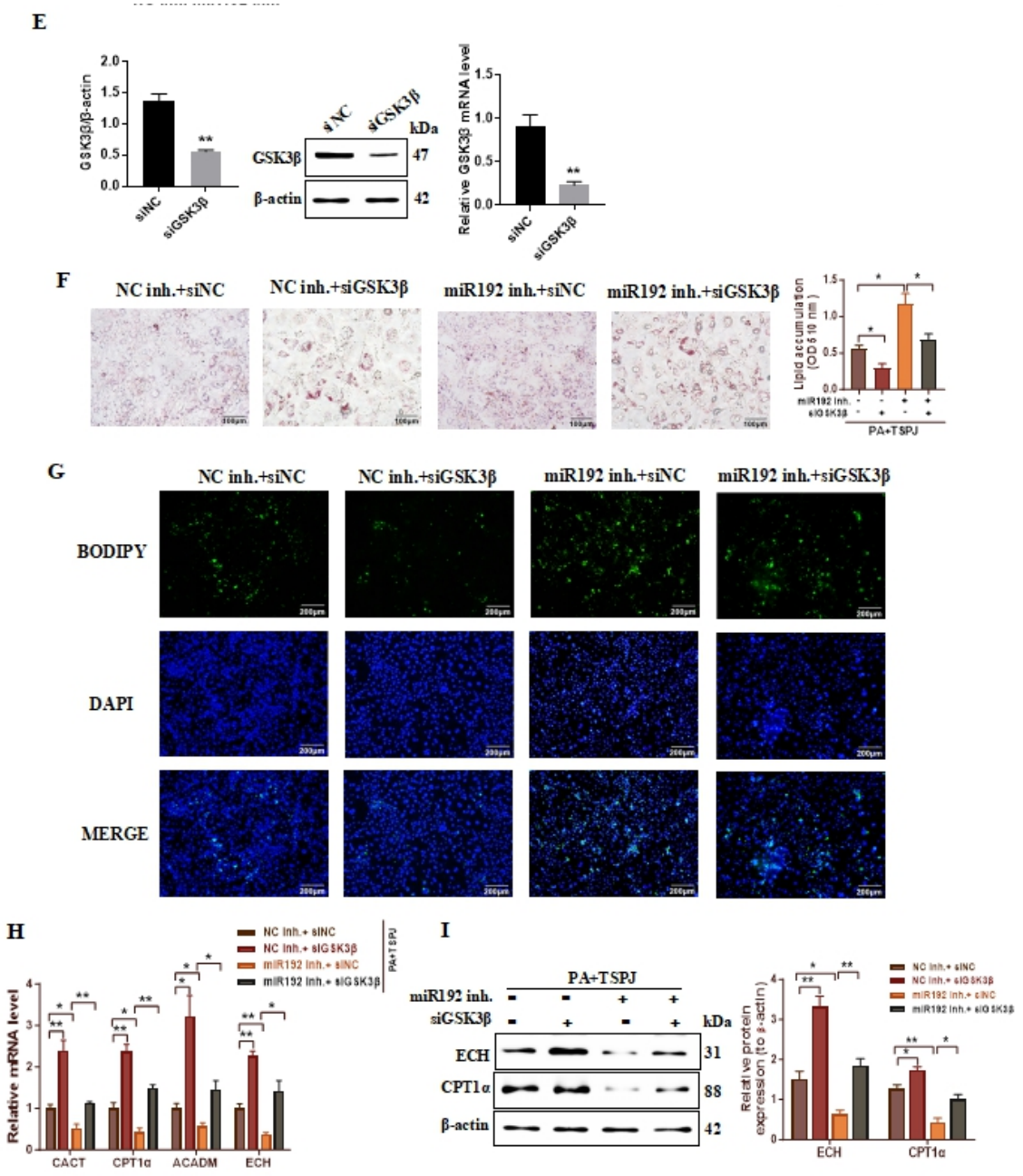

Fig. 6. TSPJ promote β-oxidation by up-regulating miR-192 and inhibiting GSK3β expression.

(A) The mRNA expression of GSK3β in 3T3-L1 cells. (B) The protein levels of GSK3β and p-GSK3β^{Ser9} in 3T3-L1 cells. (C) The mRNA expression of GSK3β in 3T3-L1 cells with miR-192 knockdown. (D) The protein levels of GSK3β and p-GSK3β^{Ser9} in 3T3-L1 cells with miR-192 knockdown. (E) The effectiveness of GSK3β knockdown. (F) Oil red O staining images and OD values of 3T3-L1 cells with GSK3β and/or miR-192 knockdown. (G) BODIPY staining of 3T3-L1 cells with GSK3β and/or miR-192 knockdown. (H) The mRNA expression levels of CACT, CPT1α, ACADM, and ECH. (I) The protein levels of CPT1α and ECH. Data are expressed as mean ± SEM (n = 8). * $P < 0.05$, ** $P < 0.01$, *** $P < 0.001$; ns, not significant.

To explore the underlying biomolecular mechanisms, additional experiments were carried out using 3T3-L1 cells with GSK3β silencing. The GSK3β expression was effectively suppressed in the 3T3-L1 cells upon the transfection of siGSK3β (Fig. 6E). For the cells induced by PA and treated with TSPJ, those transfected with siGSK3β had smaller and fewer lipid droplets, and the OD values in the oil red O test dropped (Fig. 6F). The miR-192 inhibitor had the opposite effects compared to TSPJ; when the cells had the dual knockdown of miR-192 and GSK3β, they exhibited fewer and smaller lipid droplets, and the OD values

decreased (Fig. 6F). According to BODIPY staining, the GSK3β knockdown significantly reduced lipid droplets in the adipocytes, but the miR-192 knockdown significantly increased lipid droplets. The dual knockdown of miR-192 and GSK3β significantly decrease the lipid droplets compared to when the cells only had miR-192 knockdown (Fig. 6G). Hence, the double knockdown of miR-192 and GSK3β mitigated the lipid accumulation caused by miR-192 knockdown.

The mRNA expressions of the genes encoding key β-oxidation enzymes (CACT, CPT1α, ACADM, and ECH) in the cell models were also analyzed. Their expressions were significantly upregulated by GSK3β knockdown and downregulated by miR-192 knockdown. Fig. 6H shows that the miR-192 and GSK3β double knockdown increased the mRNA expressions of these genes compared to when the cells only had miR-192 knockdown. The protein levels of CPT1α and ECH were tested by Western blot, and the same trend was observed (Fig. 6I). Therefore, miR-192 must have enhanced β-oxidation through targeting GSK3β. In sum, TSPJ facilitated β-oxidation in adipocytes by upregulating miR-192 to inhibit GSK3β expression and promote GSK3β phosphorylation.

4. Discussion

Hyperlipidemia is a major feature of diet-induced obesity and is closely linked to dysregulated adipocyte lipid handling, including excessive triglyceride storage and impaired fatty acid utilization[3, 40]. Traditional Chinese Medicine (TCM) plays a significant role in managing metabolic disorders, and we previously found that TSPJ can reduce blood lipids and mitigate fatty liver. However, whether TSPJ directly modulates adipocyte lipid metabolism, particularly fatty acid utilization/β-oxidation, and the underlying regulatory mechanism remain unclear. Therefore, this study investigated the effects of TSPJ on adipocyte lipid accumulation and fatty acid catabolism, aiming to provide mechanistic evidence supporting its potential application in obesity-associated dyslipidemia.

β-oxidation is a key pathway for fatty acid catabolism and is critical for maintaining lipid homeostasis, as insufficient β-oxidation can contribute to lipid accumulation and dyslipidemia[13, 17]. Promoting β-oxidation represents a therapeutic strategy to alleviate lipid metabolic dysregulation. Hu et al. demonstrated that the polysaccharides from *Pyracantha coccinea* can effectively reduce the body weight of obese mice and alleviate dyslipidemia by promoting the transport of fatty acids into mitochondria and enhancing mitochondrial β-oxidation and ketone body production[41]. Gimeno-Mallench et al. reported that resveratrol can improve lipid metabolism in mice by activating fatty acid mobilization[42]. The impact of TSPJ on β-oxidation in adipocytes has not been reported, although we previously found that TSPJ can reduce the serum lipid levels in HFD mice.

The current study suggested that TSPJ might strengthen β-oxidation to enhance the catabolism of FFAs. The reduction of the serum triglyceride content in HFD mice due to TSPJ was accompanied by a decrease, rather than an increase, of the levels of FFAs, which are the hydrolysis products of triglyceride (Fig. 1C-D). In addition, TSPJ markedly elevated the levels of serum β-HB, which is the most abundant ketone body in the bloodstream. According to Western blot and real-time PCR analyses, TSPJ promoted the

mRNA and protein expressions of key enzymes involved in β-oxidation (e.g., CPT1a, CACT, ACADM, and ECH) in the eWAT (Fig. 1E). In cellular models, TSPJ reduced the accumulation of lipid droplets caused by PA induction (Fig. 2A-B) and promoted the mRNA and protein expressions of key enzymes involved in β-oxidation. It could be inferred that TSPJ did not just inhibit lipid accumulation but actively enhanced mitochondrial fatty acid β-oxidation in adipocytes. Because the adipose tissue is a major source of circulating FFAs, strengthening β-oxidation in adipocytes is expected to attenuate ectopic lipid deposition and ultimately improve systemic lipid homeostasis.

miR-192 has been implicated in lipid metabolism and lipid accumulation in metabolic disease models[43]. Hu et al. found that, in obese murine models, the levels of miR-192 in the adipose tissue are lower and upregulating miR-192 can mitigate lipid accumulation in adipocytes[36]. Ma et al. demonstrated that miR-192 alleviates fatty liver in hepatocytes and its inhibitor increases serum triglyceride levels and promotes steatosis. In this work, we found that miR-192 expression was dramatically reduced in the epididymal adipose tissue of HFD mice and in PA-induced adipocytes and the TSPJ treatment increased miR-192 expression. Using models with miR-192 knockdown, we also demonstrated that miR-192 was essential in the regulation of β-oxidation in adipocytes by TSPJ. In the mouse models, the miR-192 knockdown increased the body weight, epididymal fat index and adipocyte area, whereas the TSPJ treatment had the opposite effects. For the mice receiving TSPJ, the introduction of miR-192 knockdown increased the relevant indexes (Fig. 3E-F). In the absence of miR-192 knockdown, TSPJ decreased the FFA content and increased the β-HB content, which implied enhanced β-oxidation of FFA. However, when the mice both had miR-192 knockdown and received TSPJ, the FFA content in serum was increased and the β-HB content was decreased (Fig. 3I-J). That is, TSPJ promoted β-oxidation in HFD mice and mitigated hyperlipidemia by upregulating miR-192 expression. The results from the cell models also demonstrated that TSPJ mitigated lipid deposition in adipocytes by upregulating miR-192 (Fig. 4C-D). For both animal and cell models, the introduction of miR-192 knockdown to the models treated with TSPJ substantially decreased the mRNA and protein expressions of key enzymes involved in β-oxidation.

miRNAs modulate post-transcriptional gene expression through sequence-specific interactions. Yang et al. reported that after the overexpression of miR-192-3p, there was no significant change in the mRNA level of GSK3β but p-GSK3β was significantly reduced, which led to increased degradation of β-catenin[44]. The enhanced phosphorylation of GSK3β can modulate mitochondrial function to influence lipid uptake and storage, and GSK3β knockdown has been shown to ameliorate lipid metabolism disorders. In this work, we also verified GSK3β as a downstream target of miR-192. The dual-luciferase reporter gene assay indicated that miR-192 bound to the 3' untranslated region (3'-UTR) of GSK3β and downregulated GSK3β expression at the post-transcriptional level (Fig. 5F). In the adipocytes with miR-192 knockdown, there was an increase in GSK3β expression and a decrease in the level of p-GSK3β^{Ser9}. However, in both animal and cell models, the TSPJ treatment reduced GSK3β expression and increased the level of p-GSK3β^{Ser9}. Introducing miR-192 knockdown to the models treated with TSPJ increased GSK3β expression and reduced the p-GSK3β^{Ser9}

levels (Fig. 5G-H). These findings suggested that TSPJ upregulated miR-192 to inhibit GSK3β expression and enhance the phosphorylation of GSK3β.

To determine if TSPJ modulated lipid deposition in adipocytes via the miR-192/GSK3β signaling axis, the effect of TSPJ on β-oxidation was subsequently investigated with the silencing of GSK3β. The GSK3β knockdown significantly attenuated lipid accumulation in the PA-induced 3T3-L1 adipocytes treated with TSPJ. Moreover, the dual knockdown of miR-192 and GSK3β reversed the lipid accumulation caused by the miR-192 inhibitor, implying that miR-192-3p inhibited lipid accumulation in adipocytes by targeting GSK3β (Fig. 6F). That is, TSPJ could alleviate lipid accumulation in adipocytes by regulating the miR-192/GSK3β pathway. The real-time PCR and Western blot analyses also revealed that the miR-192 knockdown reduced the expression of key enzymes involved in β-oxidation, whereas the GSK3β knockdown enhanced the expression of those key enzymes. The dual knockdown of miR-192 and GSK3β reversed the observed inhibition of key β-oxidation enzymes when the miR-192 inhibitor was applied alone (Fig. 6H). These findings suggested that miR-192 enhanced the expression of β-oxidation key enzymes by targeting GSK3β.

In summary, TSPJ promoted β-oxidation in adipocytes and mitigated lipid metabolism disorder by upregulating miR-192, thus inhibiting the expression of GSK3β and promoting its phosphorylation. The reduced levels of GSK3β enhanced the expression of key β-oxidation enzymes, which eventually relieved hyperlipidemia. However, the present study has certain limitations. The findings are based on animal models and cell experiments, and validation through clinical sample studies is needed to ensure broader applicability. Additionally, further research is needed to identify other potential targets and regulatory mechanisms of the miR-192/GSK3β pathway. These efforts could establish a stronger scientific foundation for the development of innovative treatment strategies.

5. Conclusions

This study demonstrated that TSPJ, the bioactive component of *Panax japonicus* (T. Nees) C.A. Mey., could effectively enhance β-oxidation in adipocytes through the miR-192-3p/GSK3β pathway. Specifically, TSPJ upregulated miR-192-3p to suppress the expression of GSK3β and enhance the Ser9 phosphorylation of GSK3β, which in turn activated key β-oxidation enzymes (e.g., CPT1A, PPARα) and alleviated hyperlipidemia. These findings revealed a miR-192-3p/GSK3β-dependent mechanism underlying the hypolipidemic effects of TSPJ and offered a therapeutic rationale for addressing metabolic disorders. In our future research, we intend to validate this axis in human cohorts with dyslipidemia to further understand the comprehensive effects of TSPJ and potential therapeutic applications.

Data availability statement

Additional data are available from the corresponding author upon appropriate request.

Conflict of interest

The authors declare no conflict of interest.

Acknowledgments

This work was supported by the grants from National Natural Science Foundation of China (No. 82374107 to C.F. Yuan), Chutian Talents Program Science and Technology Innovative Project of Hubei Province, Scientific Research Project on Traditional Chinese Medicine of Hubei Provincial Administration of Traditional Chinese Medicine (No. ZY2025D023 to C.F. Yuan), and Natural Science Foundation of Hubei Province (No. 2025AFB071 to Q.Q. Yao).

References

1. Anstee QM, Reeves HL, Kotsiliti E, et al., From NASH to HCC: current concepts and future challenges, Nat Rev Gastroenterol Hepatol. 16(2019) 411-428.https://doi.org/10.1038/s41575-019-0145-7.
2. Brunham LR, Familial hypercholesterolemia-Plus: is the metabolic syndrome changing the clinical picture of familial hypercholesterolemia?, Curr Opin Lipidol. 35(2024) 219-221.https://doi.org/10.1097/MOL.0000000000000938.
3. Pirillo A, Casula M, Olmastroni E, et al., Global epidemiology of dyslipidaemias, Nat Rev Cardiol. 18(2021) 689-700.https://doi.org/10.1038/s41569-021-00541-4.
4. Organization WH. Cardiovascular diseases (CVDs): World Health Organization; 2025 [Available from: https://www.who.int/news-room/fact-sheets/detail/cardiovascular-diseases-%28cvds%29.
5. Su X, Cheng Y, Zhang G, et al., Novel insights into the pathological mechanisms of metabolic related dyslipidemia, Mol Biol Rep. 48(2021) 5675-5687.https://doi.org/10.1007/s11033-021-06529-0.
6. Xu K, Saaoud F, Shao Y, et al., Early hyperlipidemia triggers metabolomic reprogramming with increased SAH, increased acetyl-CoA-cholesterol synthesis, and decreased glycolysis, Redox Biol. 64(2023) 102771.https://doi.org/10.1016/j.redox.2023.102771.
7. Eckel RH, Bornfeldt KE, Goldberg IJ, Cardiovascular disease in diabetes, beyond glucose, Cell Metab. 33(2021) 1519-1545.https://doi.org/10.1016/j.cmet.2021.07.001.
8. He Y, Jiang J, Ou L, et al., Impaired RelA signaling and lipid metabolism dysregulation in hepatocytes: driving forces in the progression of metabolic dysfunction-associated steatotic liver disease, Cell Death Discov. 11(2025) 49.https://doi.org/10.1038/s41420-025-02312-3.
9. Xu L, Yang Q, Zhou J, Mechanisms of Abnormal Lipid Metabolism in the Pathogenesis of Disease, Int J Mol Sci. 25(2024).https://doi.org/10.3390/ijms25158465.
10. Adeva-Andany MM, Carneiro-Freire N, Seco-Filgueira M, et al., Mitochondrial beta-oxidation of saturated fatty acids in humans, Mitochondrion. 46(2019) 73-90.https://doi.org/10.1016/j.mito.2018.02.009.
11. Houten SM, Wanders RJ, A general introduction to the biochemistry of mitochondrial fatty acid beta-oxidation, J Inherit Metab Dis. 33(2010) 469-477.https://doi.org/10.1007/s10545-010-9061-2.
12. Kunau WH, Dommes V, Schulz H, beta-oxidation of fatty acids in mitochondria, peroxisomes, and bacteria: a century of continued progress, Prog Lipid Res. 34(1995) 267-342.https://doi.org/10.1016/0163-7827(95)00011-9.
13. Filozof CM, Murua C, Sanchez MP, et al., Low plasma leptin concentration and low rates of fat oxidation in weight-stable post-obese subjects, Obes Res. 8(2000) 205-210.https://doi.org/10.1038/oby.2000.23.
14. Fritzen AM, Lundsgaard AM, Kiens B, Tuning fatty acid oxidation in skeletal muscle with dietary fat and exercise, Nat Rev Endocrinol. 16(2020) 683-696.https://doi.org/10.1038/s41574-020-0405-1.
15. Rogge MM, The role of impaired mitochondrial lipid oxidation in obesity, Biol Res Nurs. 10(2009) 356-373.https://doi.org/10.1177/1099800408329408.
16. Rupasinghe HP, Sekhon-Loodu S, Mantso T, et al., Phytochemicals in regulating fatty acid beta-oxidation: Potential underlying mechanisms and their involvement in obesity and weight loss, Pharmacol Ther. 165(2016) 153-163.https://doi.org/10.1016/j.pharmthera.2016.06.005.

17. Simoneau JA, Veerkamp JH, Turcotte LP, et al., Markers of capacity to utilize fatty acids in human skeletal muscle: relation to insulin resistance and obesity and effects of weight loss, FASEB J. 13(1999) 2051-2060.https://doi.org/10.1096/fasebj.13.14.2051.
18. Abdul-Rahman T, Bukhari SMA, Herrera EC, et al., Lipid Lowering Therapy: An Era Beyond Statins, Curr Probl Cardiol. 47(2022) 101342.https://doi.org/10.1016/j.cpcardiol.2022.101342.
19. Masana L, Ibarretxe D, New drugs for treating dyslipidemias. From small molecules to small interfering RNAs, Clin Investig Arterioscler. 36 Suppl 1(2024) S15-S23.https://doi.org/10.1016/j.arteri.2024.07.004.
20. Batchuluun B, Pinkosky SL, Steinberg GR, Lipogenesis inhibitors: therapeutic opportunities and challenges, Nat Rev Drug Discov. 21(2022) 283-305.https://doi.org/10.1038/s41573-021-00367-2.
21. Houten SM, Violante S, Ventura FV, et al., The Biochemistry and Physiology of Mitochondrial Fatty Acid beta-Oxidation and Its Genetic Disorders, Annu Rev Physiol. 78(2016) 23-44.https://doi.org/10.1146/annurev-physiol-021115-105045.
22. Dandare A, Khan MJ, Naeem A, et al., Clinical relevance of circulating non-coding RNAs in metabolic diseases: Emphasis on obesity, diabetes, cardiovascular diseases and metabolic syndrome, Genes Dis. 10(2023) 2393-2413.https://doi.org/10.1016/j.gendis.2022.05.022.
23. Zong Y, Wang X, Cui B, et al., Decoding the regulatory roles of non-coding RNAs in cellular metabolism and disease, Mol Ther. 31(2023) 1562-1576.https://doi.org/10.1016/j.ymthe.2023.04.012.
24. Wu S, Tang W, Liu L, et al., Obesity-induced downregulation of miR-192 exacerbates lipopolysaccharide-induced acute lung injury by promoting macrophage activation, Cell Mol Biol Lett. 29(2024) 36.https://doi.org/10.1186/s11658-024-00558-w.
25. Mysore R, Zhou Y, Sadevirta S, et al., MicroRNA-192* impairs adipocyte triglyceride storage, Biochim Biophys Acta. 1861(2016) 342-351.https://doi.org/10.1016/j.bbalip.2015.12.019.
26. Chartoumpekis DV, Zaravinos A, Ziros PG, et al., Differential expression of microRNAs in adipose tissue after long-term high-fat diet-induced obesity in mice, PLoS One. 7(2012) e34872.https://doi.org/10.1371/journal.pone.0034872.
27. Beurel E, Grieco SF, Jope RS, Glycogen synthase kinase-3 (GSK3): regulation, actions, and diseases, Pharmacol Ther. 148(2015) 114-131.https://doi.org/10.1016/j.pharmthera.2014.11.016.
28. Wang L, Li J, Di LJ, Glycogen synthesis and beyond, a comprehensive review of GSK3 as a key regulator of metabolic pathways and a therapeutic target for treating metabolic diseases, Med Res Rev. 42(2022) 946-982.https://doi.org/10.1002/med.21867.
29. Faulds KJ, Egelston JN, Sedivy LJ, et al., Glycogen synthase kinase-3 (GSK-3) activity regulates mRNA methylation in mouse embryonic stem cells, J Biol Chem. 293(2018) 10731-10743.https://doi.org/10.1074/jbc.RA117.001298.
30. Nakamura M, Liu T, Husain S, et al., Glycogen Synthase Kinase-3alpha Promotes Fatty Acid Uptake and Lipotoxic Cardiomyopathy, Cell Metab. 29(2019) 1119-1134 e1112.https://doi.org/10.1016/j.cmet.2019.01.005.
31. Papadopoli D, Pollak M, Topisirovic I, The role of GSK3 in metabolic pathway perturbations in cancer, Biochim Biophys Acta Mol Cell Res. 1868(2021) 119059.https://doi.org/10.1016/j.bbamcr.2021.119059.
32. Wang Z, Ge Y, Bao H, et al., Redox-sensitive glycogen synthase kinase 3beta-directed control of mitochondrial permeability transition: rheostatic regulation of acute kidney injury, Free Radic Biol Med. 65(2013) 849-858.https://doi.org/10.1016/j.freeradbiomed.2013.08.169.
33. Yang K, Chen Z, Gao J, et al., The Key Roles of GSK-3beta in Regulating Mitochondrial Activity, Cell Physiol Biochem. 44(2017) 1445-1459.https://doi.org/10.1159/000485580.
34. Forster K, Richter H, Alexeyev MF, et al., Inhibition of glycogen synthase kinase 3beta prevents peroxide-induced collapse of mitochondrial membrane potential in rat ventricular myocytes, Clin Exp Pharmacol Physiol. 37(2010) 684-688.https://doi.org/10.1111/j.1440-1681.2010.05372.x.
35. Chen Y, Liu M, Wen J, et al., Panax japonicus C.A. Meyer: a comprehensive review on botany, phytochemistry, pharmacology, pharmacokinetics and authentication, Chin Med. 18(2023) 148.https://doi.org/10.1186/s13020-023-00857-y.
36. Hu Y, Wang S, Wang R, et al., Total saponins from Panax japonicus regulated the intestinal microbiota to alleviate lipid metabolism disorders in aging mice, Arch Gerontol Geriatr. 125(2024) 105500.https://doi.org/10.1016/j.archger.2024.105500.

37. Yang J, Gui Y, Zheng Y, et al., Total saponins from Panax japonicus reduced lipid deposition and inflammation in hepatocyte via PHD2 and hepatic macrophage-derived exosomal miR-463-5p, J Ethnopharmacol. 342(2025) 119376.https://doi.org/10.1016/j.jep.2025.119376.
38. He YM, Lu KM, Yuan D, et al., [Studies on preparative technology and quantitative determination for extracts of total saponin in roof of Panax japonicus], Zhongguo Zhong Yao Za Zhi. 33(2008) 2607-2611
39. Yao Q, Wang R, Wang H, Yuan D, et al., Total saponins from Panax japonicus alleviate insulin resistance via exosomal miR204/Elovl6-mediated adipocyte-macrophage crosstalk. Phytomedicine. 142(2025) 156748.https://doi.org/10.1016/j.phymed.2025.156748.
40. Lustig RH, Collier D, Kassotis C, et al., Obesity I: Overview and molecular and biochemical mechanisms, Biochem Pharmacol. 199(2022) 115012.https://doi.org/10.1016/j.bcp.2022.115012.
41. Hu Y, Wang R, Wang S, et al., Selenium-enriched Polysaccharides from Pyracantha fortuneana (SePFP) Ameliorated Hepatic Lipid Accumulation through Enhancing Mitochondrial Fatty Acid beta-Oxidation in Aging Mice, J Oleo Sci. 72(2023) 929-938.https://doi.org/10.5650/jos.ess23065.
42. Gimeno-Mallench L, Mas-Bargues C, Ingles M, et al., Resveratrol shifts energy metabolism to increase lipid oxidation in healthy old mice, Biomed Pharmacother. 118(2019) 109130.https://doi.org/10.1016/j.biopha.2019.109130.
43. Ren FJ, Yao Y, Cai XY, et al., Emerging Role of MiR-192-5p in Human Diseases, Front Pharmacol. 12(2021) 614068.https://doi.org/10.3389/fphar.2021.614068.
44. Yang Q, Zhuge X, Lin W, et al., Hydrogel-based miR-192 delivery inhibits the development of hepatocellular carcinoma by suppressing the GSK3beta/Wnt/beta-catenin pathway, Neoplasma. 70(2023) 555-565.https://doi.org/10.4149/neo_2023_230317N150.